Sound & Vibration 2026, 60(4), 4292.
doi: https://doi.org/10.59400/sv4292

Article

Possibility-based transfer-matrix optimization of a graded double-cavity micro-perforated partition with fuzzy parameters for broadband sound transmission loss

Yogeesh Nijalingappa[1,2,*], Naeema Darwish Khamis Al Maashari[3], Asokan Vasudevan[3], Chethana N. S.[4], Wenya Wu[5], Suleiman Ibrahim Mohammad[2,6], Mohammad Faleh Ahmmad Hunitie[7]

[1] Department of Mathematics, Government First Grade College, Tumakuru 572102, India
[2] Research Fellow, INTI International University, Nilai 71800, Malaysia
[3] Faculty of Business and Communications, INTI International University, Nilai 71800, Malaysia
[4] Department of Mathematics, Central University of Karnataka, Kalaburagi 585367, India
[5] Faculty of Business and Communications, Xingtai Vocational College of Applied Technology, Xingtai 054000, China
[6] Department of Business Administration, Business School, Al al-Bayt University, Mafraq 25113, Jordan
[7] Department of Public Administration, School of Business, University of Jordan, Amman 11942, Jordan
* **Corresponding author:** Yogeesh Nijalingappa, yogeesh.r@gmail.com

CITATION

Nijalingappa Y, Al Maashari NDK, Vasudevan A, et al. Possibility-based transfer-matrix optimization of a graded double-cavity micro-perforated partition with fuzzy parameters for broadband sound transmission loss. Sound & Vibration. 2026; 60(4): 4292. https://doi.org/10.59400/sv4292

ARTICLE INFO

Received: 16 April 2026
Revised: 7 May 2026
Accepted: 15 May 2026
Available online: 21 July 2026

Abstract: This study proposes a possibility-based transfer-matrix optimization and assessment framework for fuzzy geometric parameters in a graded double-cavity micro-perforated partition. The system consists of a front limp panel, a first air cavity, a micro-perforated panel, a second air cavity, and a back limp panel. The two cavities are graded over three equal parallel strips, so the local depths of the two cavities differ from strip to strip. Fuzzy numbers model each uncertain design quantity as a triangular fuzzy number and propagate through alpha-cuts. The acoustic model consists of explicit transfer matrices, an area-averaged transmission coefficient, and normal-incidence sound transmission loss. The specific novelty is the direct use of exact alpha-cut corner propagation inside the graded strip-wise transfer-matrix objective, where guaranteed band-average sound transmission loss, guaranteed low-band minimum, and fuzzy width are evaluated together rather than only after a deterministic design is selected. A fuzzy width penalty and guaranteed band-average transmission loss with guaranteed low-band minimum transmission loss are included in the objective function. This is analyzed with a detailed numerical study from 250 Hz to 2,000 Hz. The selected graded design realizes a guaranteed average sound transmission loss of 78.085 dB and a guaranteed low-band minimum of 41.323 dB, while the central design gives 81.425 dB and 43.406 dB, respectively. Compared with a uniform-cavity reference evaluated under the same fuzzy setting, the graded design improves the guaranteed low-band average and minimum while maintaining a comparable uncertainty width. This study focuses on mathematical formulation, tabulated numerical output, and an accessible interpretation of design rather than a long theoretical discussion.

Keywords: fuzzy mathematics; micro-perforated panel; possibility theory; graded cavity; transfer matrix; sound transmission loss; robust acoustic design

1. Introduction

Micro-perforated panels continue to be attractive, because they produce broadband dissipation without fibrous filler, can be manufactured from metal or polymer sheets, and allow to predict their acoustic performance using compact impedance equations [1–4]. When it comes to partitions and enclosures, though, final sound transmission loss is affected more than just by panel impedance. The thickness of the cavities, mass of the outer leaves, perforation ratio, hole size, and motion interaction between layers all contribute to a transmitted wave. For this reason, design rules characterized by a single resonance formula do not suffice in most cases when maximum span or robustness with respect to geometric modification becomes the target [5, 6]. Recent sound-transmission studies have also used analytical and machine-learning representations for functionally graded single- and double-layered plates and shells, showing that acoustic performance depends strongly on geometry, cavity depth, material gradation, incidence angle, and structural response representation [7,8].

Studies have reviewed multilayer and double-leaf micro-perforated systems, transfer-matrix modeling, and vibro-acoustic coupling in partition structures [9–13]. Recent mathematical models of structural response in graded and bio-inspired laminated elements further show that spatial layout and layer sequence can alter static, vibrational, and stability behavior [14–18]. Those studies indicate that a micro-perforated insert can increase transmission loss across a wide band, though the performance remains sensitive to geometry [19–23]. A small difference between the hole diameter or cavity depth can shift the local maxima and minima. Deterministic optimization can give a strong nominal curve, but it does not directly state whether the specification is guaranteed over manufacturing tolerance intervals [24]. Probabilistic methods can provide reliability indices, but they need sufficient distributional data that are often unavailable during early acoustic design [25,26]. In practice, the designer may know a nominal perforation ratio and a nominal cavity depth, but there may be no statistically validated distribution for every manufactured strip. Therefore, fuzzy mathematics and possibility theory are helpful tools for acoustic design because they describe bounded epistemic uncertainty without presuming a statistical sample population [1–6,27].

The current work employs a normal-incidence transfer-matrix model. The layered path is straightforward: front panel, first cavity, micro-perforated sheet, second cavity, and back panel. The contribution is not the introduction of a new physical layer, but the coupling of strip-wise graded cavity depths with possibility-based lower-envelope optimization of the complete transmission-loss curve [28]. In contrast to fuzzy finite-element studies that mainly propagate uncertain structural parameters through a spatial discretization, the present model keeps the layer physics in closed transfer-matrix form and evaluates all alpha-cut corner combinations for each strip and frequency. In contrast to deterministic MPP optimization, the selected geometry is judged by a guaranteed low-band floor, a band-average lower bound, and a mean fuzzy-width penalty [29, 30]. The two cavities are graded along three parallel strips, causing the local air-depth pair to differ between strips. The design parameters are the nominal cavity depths, grading factor, perforation ratio, and hole diameter. All uncertain geometric and panel quantities are treated as fuzzy numbers, while the grading factor is used as a crisp layout variable in order to isolate the role of grading. The optimization then looks for a design that raises the guaranteed low-band floor while preserving a strong average band-average transmission loss.

The mathematical structure is intentionally explicit, and each layer has a transfer matrix; the strip-wise matrices are multiplied in sequence. The transmission coefficient of each strip is then obtained from the global matrix and the characteristic impedance of air. Finally, the three strip coefficients are averaged to produce an equivalent transmission coefficient. This deterministic chain is then wrapped inside an alpha-cut loop. At each alpha level, the uncertain parameters are converted to intervals, a corner set is generated, and the lower and upper sound transmission loss envelopes are computed over the full frequency grid. This construction addresses a limitation of many earlier multilayer MPP studies: the same model simultaneously reports nominal performance, guaranteed performance, and possibility/necessity support for target acoustic requirements, which makes the result more useful for tolerance-aware design decisions [31–34].

2. Transfer-matrix model for the graded partition

2.1. Layer arrangement and strip grading

The partition is made of two limp outer panels and one internal micro-perforated panel (MPP). The layout is shown in **Figure 1**.

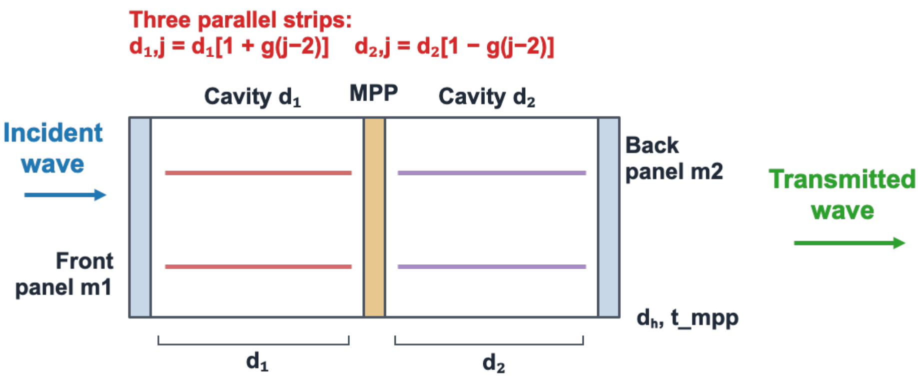

Figure 1. Graded double-cavity micro-perforated partition with fuzzy geometric parameters.

The front and back panels have surface masses m_1 and m_2. The central MPP has thickness t_{mpp}, hole diameter d_h, and perforation ratio ϕ. The two cavities are not uniform. Instead, the panel is divided into three strips of equal area fraction. The local cavity depths are:

$$d_{1,j} = d_1 \left[1 + g(j-2)\right], \qquad j = 1, 2, 3,$$

$$d_{2,j} = d_2 \left[1 - g(j-2)\right], \qquad j = 1, 2, 3,$$

where g is the grading factor. When $g = 0$, the configuration becomes a uniform double-cavity system. When $g > 0$, one strip becomes front-heavy, one remains central, and one becomes back-heavy. The purpose of grading is simple: to separate the local cavity resonances and which can reduce the concentration of transmission minima and lift the lower-band floor. The three-strip linear grading is used as the lowest-order non-uniform cavity representation that can separate shallow, central, and deep acoustic paths while keeping the number of uncertain corner evaluations manageable. Nonlinear grading, unequal strip fractions, and more than three strips are possible extensions, but they would introduce additional layout variables and obscure the main question of whether a simple graded cavity can improve the guaranteed low-band floor.

The deterministic acoustic constants used in the calculations are:

$$\rho_0 = 1.21 \text{ kg/m}^3, c_0 = 343 \text{ m/s},$$

$$Z_0 = \rho_0 c_0,\ \eta_0 = 1.84 \times 10^{-5} \text{ Pa·s}.$$

The selected nominal geometry and panel properties are listed in **Table 1**.

Table 1. Nominal physical quantities of the graded double-cavity partition.

Quantity	Value	Unit
Front limp panel mass	6.200	kg/m^2
Back limp panel mass	8.000	kg/m^2
MPP thickness	0.800	mm
Optimized nominal cavity depth $\boldsymbol{d_1}$	59.010	mm
Optimized nominal cavity depth $\boldsymbol{d_2}$	54.390	mm
Grading factor $\boldsymbol{g}$	0.180	-
Perforation ratio phi	0.877	%
Hole diameter	0.240	mm

2.2. Transfer matrices of the layers

The model uses normal-incidence plane-wave transfer matrices. For a thin limp panel with surface mass m_s and structural loss factor η_s, the specific series impedance is:

$$Z_p(\omega) = i\omega m_s \left(1 - i\eta_s\right).$$

The corresponding transfer matrix is:

$$\mathrm{T}_p = \begin{bmatrix} 1 & Z_p \\ 0 & 1 \end{bmatrix}.$$

For an air layer of depth d, the transfer matrix is:

$$\mathrm{T}_a(d) = \begin{bmatrix} \cos(kd) & iZ_0 \sin(kd) \\ iZ_0^{-1} \sin(kd) & \cos(kd) \end{bmatrix}, \qquad k = \frac{\omega}{c_0}.$$

For the thin MPP, the classical Maa-type impedance is used. The dimensionless perforation parameter is:

$$x = d_h \sqrt{\frac{\omega \rho_0}{4\eta_0}}.$$

The resistive part is written as:

$$R_{mpp} = \frac{32\eta_0 t_{mpp}}{\phi d_h^2} \left[\sqrt{1 + \frac{x^2}{32}} + \frac{\sqrt{2}}{32} x \frac{d_h}{t_{mpp}}\right],$$

and the reactive part is:

$$X_{mpp} = \omega \frac{\rho_0 t_{mpp}}{\phi} \left[1 + \frac{1}{\sqrt{9 + x^2/2}} + 0.85 \frac{d_h}{t_{mpp}}\right].$$

Hence,

$$Z_{mpp} = R_{mpp} + iX_{mpp}, \qquad \mathrm{T}_{mpp} = \begin{bmatrix} 1 & Z_{mpp} \\ 0 & 1 \end{bmatrix}.$$

Figure 2 shows the resistance and reactance of the optimized MPP. The resistance changes only mildly over the band, while the reactance rises almost linearly. This is typical of a thin perforated element with a moderate perforation ratio. The Maa impedance expression is applied within its usual linear-acoustic setting for a thin plate with circular holes and a low perforation ratio; the optimized value phi = 0.877% is well below the commonly used 5% threshold at which strong inter-hole interaction may become a concern. Because the MPP itself is not geometrically graded, the same local impedance is used in each strip, and the different backing depths enter through the neighboring cavity matrices; any higher-order cross-strip coupling or finite-panel edge interaction is therefore outside the present one-dimensional model.

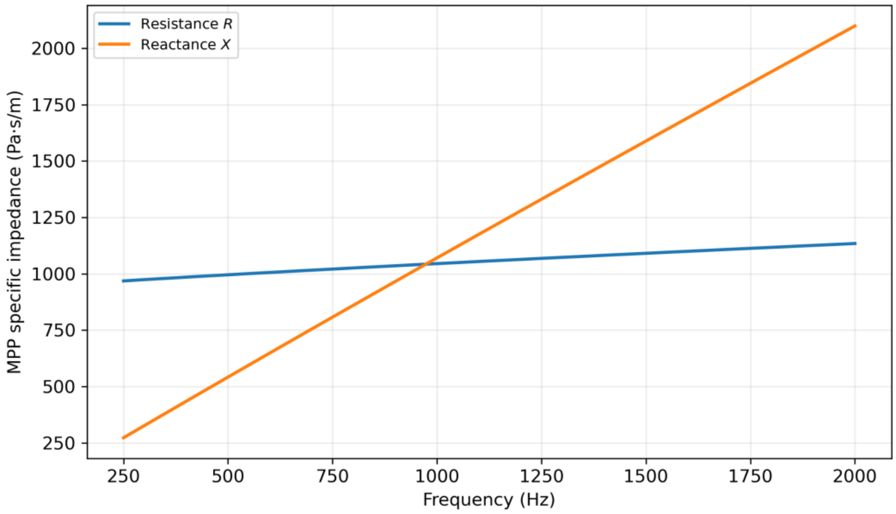

Figure 2. Maa-type impedance components of the optimized MPP.

2.3. Strip-wise transmission coefficient

For strip j, the total transfer matrix is the ordered product:

$$\mathrm{T}_j = \mathrm{T}_{p,1}\mathrm{T}_a\left(d_{1,j}\right)\mathrm{T}_{mpp}T_a\left(d_{2,j}\right)\mathrm{T}_{p,2}.$$

If,

$$\mathrm{T}_j = \begin{bmatrix} A_j & B_j \\ C_j & D_j \end{bmatrix},$$

the normal-incidence transmission coefficient of strip j is:

$$\tau_j = \frac{2}{A_j + B_j/Z_0 + C_jZ_0 + D_j}.$$

The three strips are taken as equal-area parallel paths, so the equivalent transmission coefficient is:

$$\tau_{eq} = \frac{1}{3}\sum\nolimits_{j=1}^{3}\tau_j.$$

The sound transmission loss of the graded partition is therefore:

$$STL(f) = -20\log_{10}\left|\tau_{eq}(f)\right|.$$

This is the deterministic forward model used throughout the paper. The detailed derivation connecting the total strip transfer matrix to the pressure transmission coefficient, equivalent graded coefficient, and final sound transmission loss expression is provided in **Appendix A**. Once the design variables are specified, the frequency curve is obtained by direct matrix multiplication. The arithmetic average of the three strip coefficients assumes equal strip areas, laterally separated acoustic paths, and negligible cross-flow between strips; this is most reasonable when the strip width is large compared with the hole diameter and the excitation can be approximated by a plane wave over the 250–2,000 Hz band. If strong lateral modes, small strip widths, or diffuse-field excitation dominate, the strip coefficients should be coupled through a two-dimensional or modal transfer formulation rather than a simple parallel average. The normal-incidence model can be extended to oblique incidence by replacing the air-layer wavenumber and characteristic impedance with their angle-dependent normal components and by integrating the resulting transmission coefficient over incidence angles for diffuse-field estimates.

3. Fuzzy parameterization and possibility measures

3.1. Fuzzy geometric variables

The uncertain variables are represented by triangular fuzzy numbers using the standard alpha-cut interpretation adopted in fuzzy structural dynamics and uncertainty propagation. For the present partition, the uncertain quantities are the front-panel mass, the back-panel mass, the nominal cavity depths, the perforation ratio, and the hole diameter:

$$\widetilde{m}_1 = (0.95m_1, m_1, 1.05m_1)\,,\ \widetilde{m}_2 = (0.95m_2, m_2, 1.05m_2)\,,$$

$$\widetilde{d}_1 = (0.9d_1, d_1, 1.1d_1)\,, \widetilde{d}_2 = (0.9d_2, d_2, 1.1d_2)\,,$$

$$\widetilde{\phi} = (0.9\phi, \phi, 1.1\phi),\ \widetilde{d}_h = (0.9d_h, d_h, 1.1d_h)\,.$$

The grading factor g is treated as a crisp design variable in the optimization stage so that the influence of geometry grading can be seen more clearly. The alpha-cut of each fuzzy variable is:

$$[p]_\alpha = \left[p^L + \alpha\left(p^C - p^L\right),\ p^U - \alpha\left(p^U - p^C\right)\right].$$

At level α, the six-dimensional box is:

$$\mathit{\Gamma}_\alpha = [m_1]_\alpha \times [m_2]_\alpha \times [d_1]_\alpha \times [d_2]_\alpha \times [\phi]_\alpha \times [d_h]_\alpha\,.$$

The lower and upper transmission-loss envelopes are defined pointwise by:

$$\underline{T}_{\alpha}(f) = \min_{\eta \in \Gamma_{\alpha}} STL(f;\eta),$$

$$\overline{T}_{\alpha}(f) = \max_{\eta \in \Gamma_{\alpha}} STL(f;\eta).$$

Again, the present study uses the exact corner set. Since there are six interval variables, the alpha-cut box contains 64 corners. The numerical ranges are intended to represent moderate early-design manufacturing tolerances: +/−5% for panel masses and +/−10% for cavity depths, perforation ratio, and hole diameter. These values are not claimed as universal production statistics; in an industrial application, they should be replaced by measured tolerance certificates or process-specific inspection data. The structural loss factor is kept crisp because the present objective is dominated by geometric tuning and MPP impedance, but uncertainty in damping can be added as an additional fuzzy coordinate when resonance-dominated data or material-test variability are available.

3.2. Guaranteed, optimistic, and width measures

The transmission-loss curves are summarized by three scalar metrics. The first is the guaranteed band-average transmission loss:

$$\overline{STL}_{\alpha}^{G} = \frac{1}{N_f} \sum\nolimits_{k=1}^{N_f} \underline{T}_{\alpha}\left(f_k\right).$$

The second is the guaranteed lower-band minimum over the low-frequency interval $[250, 900]$ Hz:

$$STL_{\alpha}^{min} = \min_{f \in [250,900]} \underline{T}_{\alpha}(f).$$

The third is the mean fuzzy width over the full band:

$$W_{\alpha} = \frac{1}{N_f} \sum\nolimits_{k=1}^{N_f} \left[\overline{T}_{\alpha}\left(f_k\right) - \underline{T}_{\alpha}\left(f_k\right)\right].$$

The optimization objective used in the paper is:

$$S(\theta) = \sum\nolimits_{j=1}^{m} w_j \left[0.45\overline{STL}_{\alpha_j}^{G} + 0.35\overline{STL}_{\alpha_j}^{G,low} + 0.35STL_{\alpha_j}^{min} - \beta W_{\alpha_j}\right],$$

with

$$\alpha_j \in \{0, 0.5, 1.0\},\ w_j = \{0.25, 0.35, 0.40\},\ \beta = 0.10.$$

The design vector is:

$$\theta = \left(d_1, d_2, g, \phi, d_h\right).$$

This objective prefers a tight uncertainty width plus a strong guaranteed low-frequency floor while maintaining a large band-average. The two 0.35 weights in the objective are there for a reason; one multiplies the guaranteed low-band average, and the other multiplies the guaranteed low-band minimum, so we do not just repeat this typographical term N times in our expression.

3.3. Possibility and necessity

Besides scalar optimization, reference to possibility measures are helpful for decision support. For a target metric Q^* and fuzzy response quantity Q, a simple alpha-cut estimate of possibility and necessity is:

$$\Pi\left(Q \geq Q^*\right) = \sup_{\alpha \in [0,1]} \left\{1 - \alpha \;:\; \overline{Q}_\alpha \geq Q^*\right\},$$

$$N\left(Q \geq Q^*\right) = \sup_{\alpha \in [0,1]} \left\{\alpha \;:\; \underline{Q}_\alpha \geq Q^*\right\}.$$

The tables below (Section 4) provide an evaluation of these measures against target band-average and target low-band minimum transmission loss levels. It thereby introduces an explicit decision-making layer: the designer sees a nominal value, but also how well the fuzzy set supports an acoustic requirement. In contrast to reliability-based design optimization, the existing possibility-based approach does not estimate a failure probability or a reliability index; rather, it poses questions of whether all values within a specific fuzzy support satisfy a target and at what level this support occurs. The advantage is the transparent use of bounded tolerance information when no statistical samples are available, while the drawback is that it yields not a risk estimate as a probability but a necessity/possibility statement. This difference is particularly relevant for early MPP design, when range may be known regarding the manufacture before there are sufficient measurements to easily develop a defensible probability distribution.

3.4. Numerical optimization and selected design

The search domain is:

$$d_1 \in [30, 60]\ \mathrm{mm},\ d_2 \in [30, 55]\ \mathrm{mm}, g \in [0, 0.30],\ \phi \in [0.75\%, 1.20\%],$$
$$d_h \in [0.24, 0.42]\ \mathrm{mm}.$$

The numerical search used a two-stage derivative-free procedure. In the first stage, a bounded Latin hypercube/random screening of the five central design variables was evaluated using the alpha-cut objective defined above. In the second stage, the best candidates from this screening were refined by coordinate-wise local perturbations until no further improvement of the objective was obtained within the chosen tolerance. The term optimum is therefore used in the numerical design sense of the best solution found in the stated bounded search, not as a formal proof of global optimality. Additional computational details, including the alpha-cut corner-evaluation procedure, frequency-grid implementation, numerical settings, and low-band objective mask, are summarized in **Appendix B**. A uniform reference with g = 0 was optimized under the same frequency band, fuzzy ranges, panel constants, search bounds, and objective weights, with the grading variable suppressed. The reported comparison is therefore based on the same modeling assumptions and differs only in the availability of the graded cavity layout.

$$d_1 = 59.010\,\mathrm{mm},\ d_2 = 54.390\,\mathrm{mm},\ g = 0.180,\ \phi = 0.877\%,\ d_h = 0.240\,\mathrm{mm}.$$

Its frequency responses and envelope metrics are compared with the optimized uniform reference in the next section. For reproducibility of the baseline comparison, the uniform reference used the same front-panel mass, back-panel mass, and MPP thickness as **Table 1**, with g = 0 and with d_1, d_2, phi, and hole diameter re-selected inside the same bounds before the final fuzzy evaluation.

4. Results and discussion

4.1. Comparison between graded and uniform references

The most important comparison is summarized in **Tables 2** and **3**. **Table 2** gives the alpha-cut band metrics of the selected graded design. **Table 3** compares the optimized uniform reference and the graded fuzzy design. The comparison is intended to isolate the effect of cavity grading and not a change of material system, since both designs use the same fuzzy variable definitions and the same normal-incidence acoustic constants.

Table 2. Alpha-cut metrics of the selected graded design.

Alpha	Band_avg_lower	Band_avg_upper	Low_min_lower	Low_min_upper
0.000	78.085	84.720	41.323	45.466
0.250	78.932	83.893	41.860	44.935
0.500	79.770	83.070	42.385	44.418
0.750	80.600	82.248	42.900	43.910
1.000	81.425	81.425	43.406	43.406

Table 3. Comparison between the optimized uniform reference and the selected graded fuzzy design.

Design	Guaranteed_avg	Guaranteed_min	Width_mean	Low_guaranteed_avg	Low_guaranteed_min	Central_avg	Central_min
Uniform reference	78.200	40.298	6.673	59.162	40.298	81.539	42.416
Graded fuzzy design	78.085	41.323	6.635	60.004	41.323	81.425	43.406

Three quantitative results are immediate. First, the graded design gives a guaranteed band-average transmission loss of 78.085 dB and a crisp central band average of 81.425 dB. Second, the guaranteed low-band minimum is 41.323 dB, which is higher than the corresponding value of the optimized uniform reference. Third, the mean fuzzy width is slightly smaller for the graded design, so the graded geometry also improves robustness in a small but measurable way.

The improvement is not expressed as a dramatic gain in the full-band average. Instead, the gain appears where it is needed most: the low-band floor. This aligns with the reason for the grading. The design distributes the cavity depths across strips, avoiding resonance of all local phenomena at a single frequency. So it serves to move the floor of the curve higher, rather than to lift what were already very elevated upper-band levels. This tradeoff is actually useful since it tends to be driven by the low frequencies that can still reside inside the operating band. Relative to the reference of uniform, the improvement in guaranteed low-band minimum is only 1.025 dB, but as a percentage, it is rather modest; it is meaningful if specifications are written as min-band constraints, where acceptance often hinges on an absolute guarantee in the lowest third-octave band. The interpretation of the figure is a respect to a robust-design gain in accordance with the indicated normal-incidence model and not as a universal field-installation margin.

4.2. Frequency-response curves and selected frequencies

The transmission-loss curves of the optimized uniform reference, crisp graded design, and alpha-zero support envelope of the graded design are shown in **Figure 3**. The curve is monotone upward on average, but still includes local deviations due to the panel-cavity interaction and MPP impedance. The frequency-dependent behavior of the graded central design does not always dominate that of the uniform reference. Rather, it primarily allows the lower-band floor to be raised while narrowing the edges of that fuzziness.

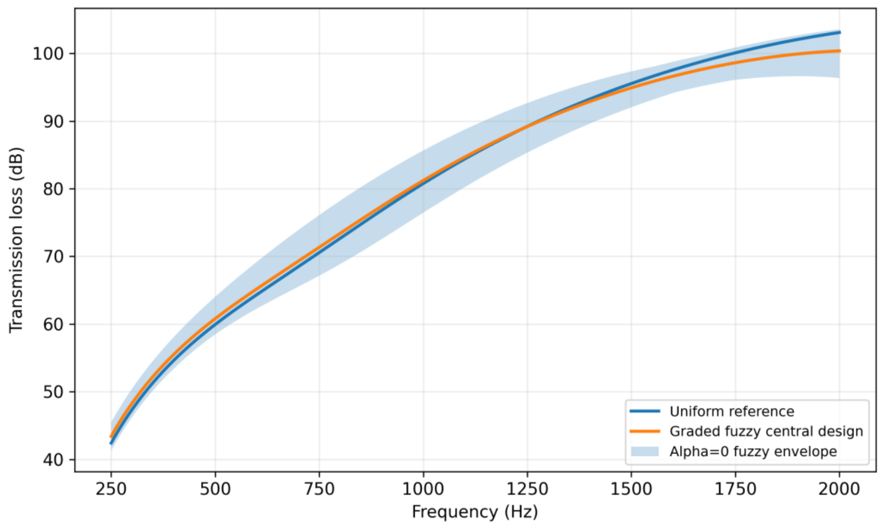

Figure 3. Normal-incidence STL of the uniform and graded fuzzy partitions.

Table 4 includes representative numerical values at selected frequencies. As the range of interest by the objective is 315 Hz to 1,000 Hz, from **Table 1** it can be seen that the graded design gives higher transmission loss than the uniform reference. The graded alpha-zero lower bound at 315, 400, 500, and 630 Hz is in clear exposition above the low-frequency floor target and therefore contributes directly to the guaranteed performance. The uniform and graded designs already have a relatively high transmission loss (>1,000 Hz) even before optimization, which means that the practical need for such improvements is lower.

The chosen-frequency table also clarifies the role of fuzziness. At high frequencies, the cavity phase rotation becomes faster, and MPP reactance increases, making the difference larger than the alpha-zero lower and upper bounds. The fairly broad band around 800 Hz is part of a local panel-cavity interaction region where small variations in d_1, d_2, phi, or hole diameter move the attenuation feature nearby. The optimistic alpha-zero upper limit of 84.720 dB is presented when the cavity-depth/hole-geometry corners shift what local attenuation characteristics exist to be more in line with what operates best across a given averaging band. However, note that the guaranteed lower bound is still strict across the entire design band, thus lending itself to the robustness of this selected geometry for a submission-level engineering study.

Table 4. Selected-frequency transmission loss values for the uniform reference and the graded fuzzy design.

Frequency_hz	Uniform_reference	Graded_central	Graded_alpha0_lower	Graded_alpha0_upper
315.000	48.618	49.540	47.447	51.670
400.000	54.605	55.486	53.335	57.980
500.000	59.936	60.795	58.532	64.092
630.000	65.596	66.438	63.282	70.636
800.000	72.656	73.390	68.834	78.181
1,000.000	80.764	81.214	76.495	85.671
1,250.000	89.209	89.186	85.312	92.632
1,600.000	97.552	96.623	94.139	98.747
2,000.000	103.084	100.362	96.361	103.561

4.3. Contour map of grading and perforation ratio

The quantified low-band average transmission loss is presented as a function of the grading factor and perforation ratio in **Figure 4**, where other nominal quantities maintain constant values from those chosen previously. The contour map has a couple of important properties. First, the smooth surface of performance. Second, the maximum is in the mid-region rather than at the edge of the design box. This implies that the design is not forced to meet a hard bound. The selected design point, g = 0.18 and phi = 0.877%, is marked on the contour map and lies inside the interior high-performance region rather than on the boundary of the design space.

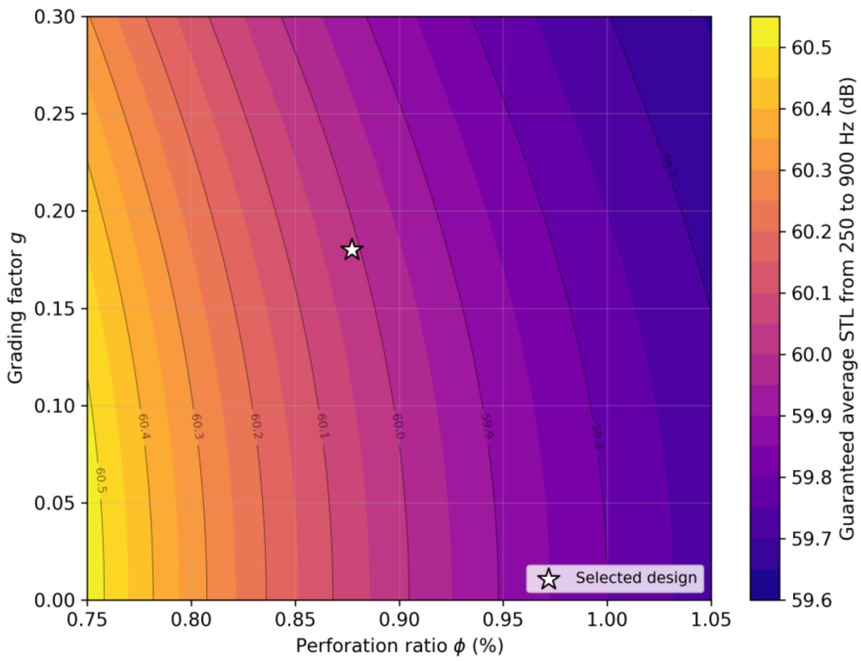

Figure 4. Guaranteed low-band average STL over perforation ratio and grading factor.

The map gives a simple physical interpretation. If the perforation ratio is too low, the MPP becomes overly reactive, and the low-band benefit diminishes. For an extremely permeable structure, the resistive term fades and the broadband effect is weakened. The same trade-off occurs with the grading input. A g which is small enough behaves like a uniform cavity, but if g is too large, it decouples the local cavity lengths so strongly that this can diminish the average response. The chosen design is therefore not an extreme point but an interior compromise. A separate depth-depth contour is not added in this revision to keep the manuscript concise, but **Table 5** and the sensitivity discussion identify d_2 as the more influential of the two cavity-depth variables for the selected geometry.

Table 5. Local normalized sensitivities of the possibility-based objective.

Parameter	dS_dtheta	Normalized_sensitivity
hole	−36807.136	0.078
phi	−829.101	0.064
d_2	129.767	0.062
d_1	94.195	0.049
g	−4.471	0.007

4.4. Alpha-cut evolution of band metrics

We see in **Figure 5** that the fuzzy acoustic metrics contracted across the alpha levels. At alpha zero, the guaranteed band average is 78.085 dB, and it rises to 81.425 dB at alpha one. The minimum across the low-band for guaranteeing a signal has increased from 41.323 dB to 43.406 dB in this case. Simultaneously, the band average goes down toward the same crisp value in an optimistic manner. This nested behavior is both expected and desirable.

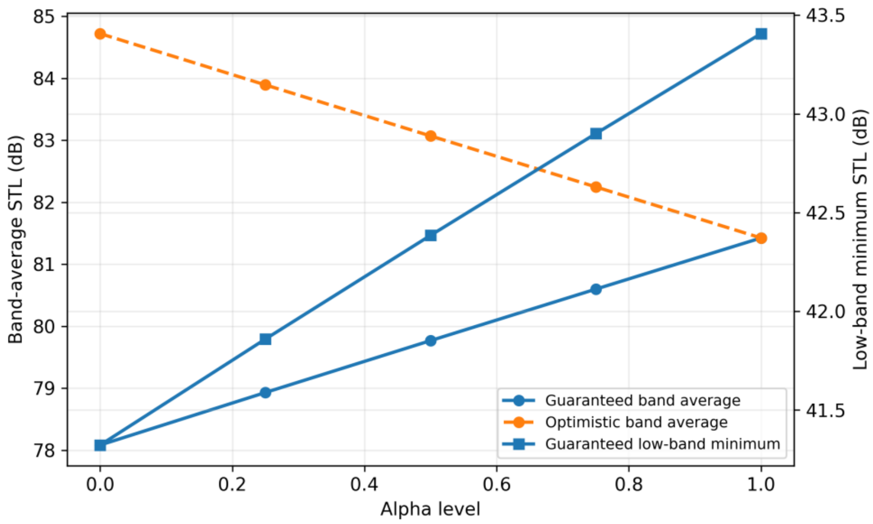

Figure 5. Alpha-cut evolution of the average and guaranteed minimum STL.

The alpha-cut trends also make the possibility interpretation easy. If the design requirement is modest, both possibility and necessity will be high. If the design requirement is severe, possibility may still be high while necessity falls. This is exactly the type of graded information that a deterministic design cannot provide. Instead of a single yes-or-no answer, the fuzzy model gives a range of support for each target acoustic requirement. The monotonic contraction with alpha also confirms that the triangular fuzzy model behaves consistently: alpha = 0 represents the widest admissible tolerance box, alpha = 1 is the central crisp design, and intermediate alpha levels provide nested degrees of support for design claims.

4.5. Sensitivity ranking of the design variables

The local sensitivity results are given in **Table 5** and **Figure 6**. The derivatives in **Table 5** were computed at the crisp selected design using normalized one-at-a-time perturbations of the central variables; they therefore measure local design sensitivity, not an average over every alpha-cut corner.

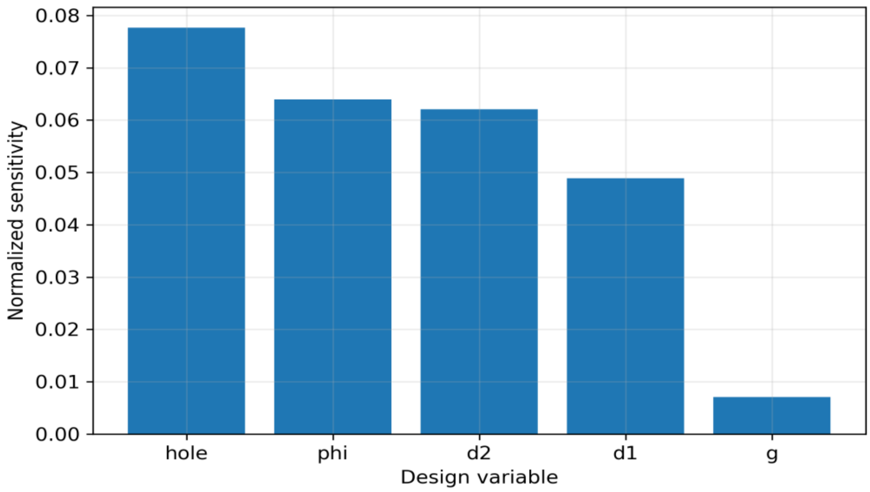

Figure 6. Sensitivity ranking for the possibility-based objective.

The hole diameter is the most sensitive variable, followed by perforation ratio and the second cavity depth. This ranking is physically reasonable. Both hole diameter and perforation ratio enter the MPP impedance directly. A small change in these quantities changes the balance of resistance and reactance in every strip. The second cavity depth is slightly more influential than the first cavity depth in the present design because the selected grading arrangement places a larger part of the low-band tuning burden on the downstream cavity. A supplementary alpha-level check showed the same leading variables across the tested alpha levels, although the relative influence of d_2 becomes closer to phi at wider uncertainty supports because cavity-depth perturbations shift the low-band interaction region.

The grading factor has the smallest local sensitivity near the selected design. This result does not imply that grading is irrelevant; rather, once a moderate interior value of g has been selected, small local perturbations in g change the objective less than comparable relative perturbations in hole geometry. From a manufacturing viewpoint, this is useful because the low-band floor can be improved without requiring extremely tight grading tolerances.

5. Possibility and necessity results

Table 6 reports the possibility and necessity estimates for several target metrics.

Table 6. Possibility and necessity estimates for target acoustic requirements.

Target	Possibility	Necessity
Band average ≥ 80 dB	1.000	0.569
Band average ≥ 80.5 dB	1.000	0.720
Low-band minimum ≥ 43 dB	1.000	0.799
Low-band minimum ≥ 44 dB	0.294	0.000

Table 6 provides a decision-oriented comparison. For the target "band average at least 80 dB," both possibility and necessity are high, indicating that the design strongly supports this target. For "band average at least 80.5 dB", is also achievable; however, the support becomes more selective since a higher alpha level would need to be used for the lower envelope to break above the threshold. Thus, the possibility is strictly positive but necessity is zero for the target "low-band minimum at least 44 dB," meaning that it is theoretically possible to hit target values with favorable fuzzy parameter configurations, but those targets will not be guaranteed over the whole support. In order to increase the need above zero to hit 44 dB, either uncertainty in hole diameter and perforation ratio must be reduced, the maximum low-band tuning margin adjusted by slightly reducing d_1 and d_2, or the mass of the panel added (where weight constraints allow). This information is useful because it allows the designer to choose between improved manufacturing control and a more conservative acoustic geometry instead of relying on a single nominal value.

5.1. Engineering interpretation

The graded design operates by redistributing resonance conditions. In a uniform double cavity, we have the same pair of cavity depths appearing in all three area fractions, so that local resonant interactions are saturating. In the graded design,

$$(d_{1,1}, d_{2,1}) \neq (d_{1,2}, d_{2,2}) \neq (d_{1,3}, d_{2,3}),$$

this expands the conditions of the acoustic path. The equivalent transmission coefficient,

$$\tau_{eq} = \frac{\tau_1 + \tau_2 + \tau_3}{3},$$

so the averaged path is less likely to experience a simultaneous low-transmission weakness in all strips. To put it differently, grading does not really raise the top of the curve: It raises the bottom of the curve.

This interpretation is consistent with the findings of these numerical results. The full-band average is slightly greater for the uniform reference, however, both the guaranteed low-band average and the guaranteed low-band minimum are larger for the graded pattern. Full-band average does not always require such a large increase because often the weakest frequency band controls practical acoustic specifications. Thus, a small increment in the guaranteed low-band floor can be important as long as the design must meet minimum-band requirements.

An ideal design track might be expressed as a repeatable engineering process. For each outer layer of the panel, you have to select a mass from structural bound or MPP thickness, which is possible by fabrication. Second, set feasible tolerances on d_1, d_2, phi and hole diameter. Third, calculate a uniform reference: $g = 0$ to establish the low-band floor. Fourth, the fuzzy objective is expanded to include a modest grading factor within an acceptable range (commonly based in the middle of the available range) with re-optimization of cavity depths and MPP geometry. Lastly, assess the target levels you have chosen with the help of the possibility and necessity table. The whole workflow is straightforward, clear, and can be reproduced.

5.2. Strip-wise phase separation and practical sizing notes

A useful way to interpret the graded partition is to look at the complex strip coefficients rather than only their magnitudes. Write,

$$\tau_j(f) = |\tau_j(f)|\, e^{i\psi_j(f)}.$$

Then the equivalent transmission coefficient is:

$$\tau_{eq}(f) = \frac{1}{3}\left[|\tau_1|\, e^{i\psi_1} + |\tau_2|\, e^{i\psi_2} + |\tau_3|\, e^{i\psi_3}\right].$$

This means that in a uniform partition, where all the cavities have identical lengths, these first three phases are almost indistinguishable. This indicates that the sum acts like three identical copies of a path. However, in the graded partition, the phases are different due to differences in acoustic travel lengths. The amplitude of the average sum is defined by strip amplitudes, assigned with phase offsets. So the grading works through two means: it changes the local resonant magnitudes and it alters how strip responses sum.

This can be approximated crudely, but in a useful way, by taking the equivalent size and squaring it:

$$|\tau_{eq}|^2 = \tfrac{1}{9}[|\tau_1|^2 + |\tau_2|^2 + |\tau_3|^2 + 2\,|\tau_1|\,|\tau_2| \cos(\psi_1 - \psi_2)$$
$$+2\,|\tau_1|\,|\tau_3| \cos(\psi_1 - \psi_3) + 2\,|\tau_2|\,|\tau_3| \cos(\psi_2 - \psi_3)].$$

That form is useful because it illustrates in a straightforward way why the graded design does NOT collapse to a single strip resonance. The need for the total response to be low domain can remain strong when one strip has a local curve of response. That same equation explains why overly aggressive grading is also a bad idea. But if the individual strip phases separate too much, then the average response may degrade, because one path ends up being acoustically inefficient over a larger part of the band. One useful guideline for the current range of numerical simulations is that you should start with a g value between 0.10 and 0.22, set d_1 and d_2 at around ~50–60 mm, then adjust the hole diameter before making larger adjustments to the grading factor. This rule should be taken as something to start from rather than an alternative to final alpha-cut validation.

From a size point of view, the geometry we chose is Front cavity depth, nominal < 60 mm Back cavity depth, nominal ~54 mm Grading factor 0.18 There are about 3 pairs of strips:

$$(d_{1,1}, d_{2,1}) \approx (48.4, 64.2)\ \text{mm},$$

$$(d_{1,2}, d_{2,2}) \approx (59.0, 54.4) \text{ mm},$$

$$(d_{1,3}, d_{2,3}) \approx (69.6, 44.6) \text{ mm}.$$

The three paths are different enough that they can be cleanly separated when it comes to the low-frequency features, but not so different that one path becomes acoustically redundant. This is why we use the inner range of **Figure 4** to pick the information of interest as a weighted grading factor; the chosen grade will never be zero or close to it. In combination, current results recommend moderate positive grading for a target low-frequency floor near 41–43 dB (avoid extreme regions of the contour map); for a conservative 44 dB guaranteed minimum low-band lower envelope is established, hole-diameter uncertainty or retuned d_2 should be first to be reduced as these factors exert the strongest influence on the band-envelope.

This is also why we use perforation ratio and hole diameter. The ultimate design is characterised by a smaller hole diameter and a medium perforation ratio. With a low-band upgrade, the smaller hole increases resistance and inertial end correction, but one shouldn't reduce perfection too much, else the panel is “overreactive”. The optimization combines these two trends while choosing values that agree with the graded lengths of the cavity.

In practice, this phase-based interpretation is convenient since it translates a fuzzy design process into a strict engineering rule. Apply a positive grading factor to compensate for low-frequency floor performance alone with a small hole diameter and a small perforation ratio if the specification is controlled by low frequency. The most maximally full-band average dominant specification may allow the design to retake its recourse towards a more uniform cavity. Consequently, the present analysis not only produces a unique overall numerical optimum but also provides a readable specification of how the shape should change as design priorities shift. The qualitative principle of grading should also hold in the more complicated case where diffuse-field or oblique-incidence data are needed, but d_1, d_2 and g values should be re-optimized after integration over angles (which changes effective cavity phase lengths). The numerical results can be expressed as a tuning rule step by step for engineering use directly. When the guaranteed minimum falls short of the desired low-band floor, then we should start by reducing hole-diameter uncertainty or nominal hole diameter a little because this variable has the highest normalized sensitivity. Supposing that at the end of this correction, the low-band average is coherent with a lower-than-expected cavity phase for channel d2, it should be tuned next as it shifts down all features upstream from this transmission peak and then provides additional adjustment to the normal location of this dominant new feature on the spectrogram. The grading factor must then be shifted only a little, since values close to zero bring back a non-graded cavity, and high values separate the paths too much. This sequence of work is consistent with the sensitivity table, contour map, and impact results but also provides a simple idea of what could be a working design before going through the expensive process of re-optimization.

The present work is a theoretical and numerical design study. Direct experimental validation for the exact graded double-cavity fuzzy MPP partition was not available during this revision, so confidence is based on the use of established transfer matrices, the Maa-type impedance model, and comparison with the behavior reported for multilayer MPP and sound-transmission studies. A practical validation route would be to fabricate the three-strip partition, measure normal-incidence STL in an impedance-tube or four-microphone facility, and then compare measured third-octave values with the predicted central curve and alpha-zero envelope. The expected experimental tolerance should be compared with the alpha-zero support rather than only with the central curve, because the reviewer-requested robustness claim depends on whether measured samples fall inside the predicted lower and upper envelopes. If the measured curve lies systematically outside the envelope, the fuzzy ranges or the one-dimensional strip assumption should be recalibrated before using the model for final design approval.

6. Conclusion

This study formulates a hypothesis-driven mathematical framework that estimates the special influences of fuzziness attributed to geometric parameters on a double-cavity micro-perforated partition with an inhomogeneous inner cavity. It combines transfer matrices for the layered acoustic path with a Maa-type impedance model and alpha-cut propagation leading to possibility-type decision-making metrics.

The calculations were carried out over the entire 250–2,000 Hz band and confirm that the chosen graded design ensures a band-average transmission loss of 78.085 dB, as well as a guaranteed low-band minimum of 41.323 dB. The near-hub central values are 81.425 dB and 43.406 dB, respectively.

In comparison with the uniform reference, the presented graded configuration shows an advantage in an improvement of the low-band guaranteed average value and a guarantee on the minimum value expressed by a slightly smaller mean fuzzy width. Thus, the main design advantage is providing a relaxed lower-band threshold rather than a significant increase in already high upper-band transmission-loss values.

The importance of these results is that the ranking indicates which tolerances are most sensitive to variation in manufacture, with hole diameter and perforation ratio contributing more than the grading factor near to the selected design. The results of this study therefore demonstrate that fuzzy mathematics and possibility theory can offer a viable approach to resilient acoustic partition design, particularly where tolerance ranges are known but full probabilistic data cannot be obtained. Future work should explore nonuniform strip fractions, nonlinear grading, oblique incidence, diffuse-field averaging, and experimental verification of the predicted fuzzy envelopes.

Author contributions: Conceptualization, YN and AV; methodology, YN and CNS; software, YN and WW; validation, NDKAM, SIM and MFAH; formal analysis, YN and CNS; investigation, YN and NDKAM; resources, AV and SIM; data curation, WW and MFAH; writing—original draft preparation, YN; writing—review and editing, NDKAM, AV, CNS, WW, SIM and MFAH; visualization, YN and WW; supervision, AV; project administration, YN and NDKAM; funding acquisition, AV and SIM. All authors have read and agreed to the published version of the manuscript.

Funding: This work received no external funding.

Institutional review board statement: Not applicable.

Informed consent statement: Not applicable.

Data availability statement: All the data are inserted in the manuscript itself as per this study.

Conflict of interest: The authors declare no conflict of interest.

AI use statement: No AI tool was used independently for experimental measurement, raw-data collection, or final scientific decision-making. All outputs were critically reviewed and edited by the authors, who take full responsibility for the integrity and accuracy of the work.

References

1. Zadeh LA. Fuzzy sets. Information and Control. 1965; 8(3): 338–353. doi: 10.1016/S0019-9958(65)90241-X
2. Zadeh LA. Fuzzy sets as a basis for a theory of possibility. Fuzzy Sets and Systems. 1978; 1(1): 3–28. doi: 10.1016/0165-0114(78)90029-5
3. Dubois D, Prade H. Operations on fuzzy numbers. International Journal of Systems Science. 1978; 9(6): 613–626. doi: 10.1080/00207727808941724
4. Hanss M. The transformation method for the simulation and analysis of systems with uncertain parameters. Fuzzy Sets and Systems. 2002; 130(3): 277–289. doi: 10.1016/S0165-0114(02)00045-3
5. Hanss M. The Extended Transformation Method for the Simulation and Analysis of Fuzzy-Parameterized Models. International Journal of Uncertainty, Fuzziness and Knowledge-Based Systems. 2003; 11(06): 711–727. doi: 10.1142/S0218488503002491
6. Moens D, Vandepitte D. Fuzzy Finite Element Method for Frequency Response Function Analysis of Uncertain Structures. AIAA Journal. 2002; 40(1): 126–136. doi: 10.2514/2.1621
7. Jiang C, Babaei M. Machine learning-based estimation of sound transmission loss in single and double-layered rectangular functionally graded plates. Engineering Applications of Artificial Intelligence. 2025; 161: 112112. doi: 10.1016/j.engappai.2025.112112
8. Fang Z, Liu W, Asemi K. Machine learning estimation on functionally graded carbon nanotube-reinforced honeycomb sandwich shells: Sound transmission analysis. Engineering Applications of Artificial Intelligence. 2026; 167: 113672. doi: 10.1016/j.engappai.2025.113672
9. Cobo P, Simón F. Multiple-Layer Microperforated Panels as Sound Absorbers in Buildings: A Review. Buildings. 2019; 9(2): 53. doi: 10.3390/buildings9020053
10. Kim HS, Ma PS, Kim SR, et al. A model for the sound absorption coefficient of multi-layered elastic micro-perforated plates. Journal of Sound and Vibration. 2018; 430: 75–92. doi: 10.1016/j.jsv.2018.05.036
11. Kim HS, Kim SR, Kim BK, et al. Sound transmission loss of multi-layered infinite micro-perforated plates. The Journal of the Acoustical Society of America. 2020; 147(1): 508–515. doi: 10.1121/10.0000600
12. Kim HS, Ma PS, Kim BK, et al. Sound transmission loss of multi-layered elastic micro-perforated plates in an impedance tube. Applied Acoustics. 2020; 166: 107348. doi: 10.1016/j.apacoust.2020.107348
13. Putra A, Ismail AY. Normal Incidence of Sound Transmission Loss from Perforated Plates with Micro and Macro Size Holes. Advances in Acoustics and Vibration. 2014; 2014: 1–12. doi: 10.1155/2014/534569
14. Zarastvand M, Ghassabi M, Talebitooti R. Prediction of acoustic wave transmission features of the multilayered plate constructions: A review. Journal of Sandwich Structures & Materials. 2022; 24(1): 218–293. doi: 10.1177/1099636221993891
15. Li X, Liu B, Chang D. An acoustic impedance structure consisting of perforated panel resonator and porous material for low-to-mid frequency sound absorption. Applied Acoustics. 2021; 180: 108069. doi: 10.1016/j.apacoust.2021.108069
16. El Kharras B, Garoum M, Bybi A. Effect of Acoustic Enclosure on the Sound Transmission Loss of Multi-Layered Micro-Perforated Plates. Archives of Acoustics. 2024; 241–254. doi: 10.24425/aoa.2024.148781

17. Fung ML, Tang SK, Leung M. Sound transmission across a rectangular duct section with a thin micro-perforated wall backed by a sidebranch cavity. Applied Acoustics. 2024; 219: 109920. doi: 10.1016/j.apacoust.2024.109920
18. Yang W, Li Y, Choy YS. Sound radiation control of an unbaffled long enclosure using wavy micro-perforated panel absorbers. Journal of Sound and Vibration. 2024; 574: 118233. doi: 10.1016/j.jsv.2023.118233
19. Qian Y, Gao Z, Zhang J, et al. Investigation on the band narrowing and shifting effects of micro-perforated panel absorbers. The Journal of the Acoustical Society of America. 2024; 155(3): 1950–1968. doi: 10.1121/10.0025277
20. Agarwalla DK, Mohanty AR. Low-Frequency Wideband Sound Absorption Properties of Composite Layer Micro-perforated Panel Absorber. Journal of Vibration Engineering & Technologies. 2024; 12(4): 6251–6271. doi: 10.1007/s42417-023-01250-7
21. Arjunan A, Baroutaji A, Robinson J, et al. Acoustic metamaterials for sound absorption and insulation in buildings. Building and Environment. 2024; 251: 111250. doi: 10.1016/j.buildenv.2024.111250
22. Mohammadi M, Ishak MR, Sultan MTH, et al. A Comprehensive Review of Factors Influencing the Sound Absorption Properties of Micro-Perforated Panel Structures. Journal of Vibration Engineering & Technologies. 2025; 13(5): 319. doi: 10.1007/s42417-025-01849-y
23. Xie Y, Hou X, Wang L, et al. Sound absorption characteristics of micro-perforated panel-sound-absorbing sponge composite structure. Technical Acoustics. 2025; 44(5): 758–764. DOI: 10.16300/j.cnki.1000-3630.23121202 (in Chinese)
24. Chen C, Wang C, Zhao Y, et al. An isogeometric modeling and vibro-acoustic characteristics analysis of a double panel-acoustic cavity coupling system with in-plane functionally graded materials. Scientific Reports. 2025; 15(1): 6554. doi: 10.1038/s41598-025-90826-2
25. Bayat MJ, Kalhori A, Asemi K, et al. Static and vibrational characteristics of bio-inspired helicoid laminated composite annular sector plates embedded on Winkler elastic foundation. Engineering Structures. 2025; 334: 120194. doi: 10.1016/j.engstruct.2025.120194
26. Bayat MJ, Kalhori A, Babaei M, et al. Buckling Characteristics of Bio-Inspired Helicoidal Laminated Composite Spherical Shells Under External Normal and Torsional Loads Subjected to Elastic Support. Buildings. 2025; 15(17): 3165. doi: 10.3390/buildings15173165
27. Mourelatos ZP, Zhou J. Reliability Estimation and Design with Insufficient Data Based on Possibility Theory. AIAA Journal. 2005; 43(8): 1696–1705. doi: 10.2514/1.12044
28. Maa DY. Theory and Design of Microperforated Panel Sound-Absorbing Constructions. Scientia Sinica. 1975; 18(1): 55–71. Available online: https://www.sciengine.com/Math%20A0/doi/10.1360/ya1975-18-1-55
29. Maa DY. Microperforated-Panel Wideband Absorbers. Noise Control Engineering Journal. 1987; 29(3): 77. doi: 10.3397/1.2827694
30. Maa DY. Potential of microperforated panel absorber. The Journal of the Acoustical Society of America. 1998; 104(5): 2861–2866. doi: 10.1121/1.423870
31. Lee DH, Kwon YP. Estimation of the absorption performance of multiple layer perforated panel systems by transfer matrix method. Journal of Sound and Vibration. 2004; 278(4–5): 847–860. doi: 10.1016/j.jsv.2003.10.017
32. Toyoda M, Takahashi D. Sound transmission through a microperforated-panel structure with subdivided air cavities. The Journal of the Acoustical Society of America. 2008; 124(6): 3594–3603. doi: 10.1121/1.3001711
33. Sakagami K, Matsutani K, Morimoto M. Sound absorption of a double-leaf micro-perforated panel with an air-back cavity and a rigid-back wall: Detailed analysis with a Helmholtz–Kirchhoff integral formulation. Applied Acoustics. 2010; 71(5): 411–417. doi: 10.1016/j.apacoust.2009.11.014
34. Sakagami K, Fukutani Y, Yairi M, et al. A theoretical study on the effect of a permeable membrane in the air cavity of a double-leaf microperforated panel space sound absorber. Applied Acoustics. 2014; 79: 104–109. doi: 10.1016/j.apacoust.2013.12.015

Appendix A. Expanded transmission-loss formulas

For any strip j, let,

$$\mathrm{T}_j = \begin{bmatrix} A_j & B_j \\ C_j & D_j \end{bmatrix}.$$

The forward and backward pressures at the incident side and transmission side satisfy,

$$\begin{bmatrix} p_0 \\ u_0 \end{bmatrix} = \mathrm{T}_j \begin{bmatrix} p_t \\ u_t \end{bmatrix}.$$

If the medium on both sides is air, the transmitted volume velocity satisfies,

$$u_t = \frac{p_t}{Z_0}.$$

Substituting this relation into the transfer equation gives,

$$p_0 = \left(A_j + \frac{B_j}{Z_0}\right) p_t,$$

$$u_0 = \left(C_j + \frac{D_j}{Z_0}\right) p_t.$$

For a unit incident wave plus a reflected wave on the left side, one obtains the familiar transmission coefficient,

$$\tau_j = \frac{2}{A_j + B_j/Z_0 + C_j Z_0 + D_j}.$$

The equivalent graded coefficient is,

$$\tau_{eq} = \sum\nolimits_{j=1}^{3} \alpha_j \tau_j,\ \alpha_j = \frac{1}{3}.$$

Finally,

$$STL = -20 \log_{10} |\tau_{eq}|.$$

The fuzzy lower and upper envelopes follow immediately from this deterministic formula once the uncertain parameter vector is restricted to the alpha-cut box.

Appendix B. Additional notes on the optimization procedure

The graded partition model is computationally cheap. For each alpha level, the six uncertain variables generate 64 corner combinations. Each corner is evaluated on the frequency grid. The lower and upper curves are then obtained pointwise. The numerical settings used in the study may be summarized as,

$$f \in [250, 2000]\ \text{Hz},\ N_f = 600 \text{ for final curves},$$

$$\alpha \in \{0, 0.25, 0.50, 0.75, 1.00\},$$

$$N_{corners} = 64.$$

A low-band mask $f \leq 900$ Hz is used in the possibility-based objective because the lower-band floor is usually the most difficult part of the specification. The same alpha-cut machinery can easily be extended to oblique incidence or more strips, but the present normal-incidence formulation is already sufficient to reveal the main graded-cavity trends.